Annu. Rev. Phys. Chem. 2004. 55:333–61
doi: 10.1146/annurev.physchem.55.091602.094402

First published online as a Review in Advance on February 6, 2004

QUANTITATIVE PREDICTION OF CRYSTAL-NUCLEATION RATES FOR SPHERICAL COLLOIDS: A Computational Approach

Stefan Auer[1] and Daan Frenkel[2]
[1]*Department of Chemistry, Cambridge University, Lensfield Road, Cambridge, CB2 1EW, United Kingdom; email: sa372@cam.ac.uk*
[2]*FOM Institute for Atomic and Molecular Physics, Kruislaan 407, 1098 SJ Amsterdam, The Netherlands; email: D.Frenkel@amolf.nl*

Key Words crystallization rates, Monte Carlo, umbrella sampling, classical nucleation theory, nucleation barrier, kinetic prefactor

■ **Abstract** This review discusses the recent progress that has been made in the application of computer simulations to study crystal nucleation in colloidal systems. We discuss the concept and the numerical methods that allow for a quantitative prediction of crystal-nucleation rates. The computed nucleation rates are predicted from first principles and can be directly compared with experiments. These techniques have been applied to study crystal nucleation in hard-sphere colloids, polydisperse hard-sphere colloids, weakly charged or slightly soft colloids, and hard-sphere colloids that are confined between two-plane hard walls.

1. INTRODUCTION

Heating a block of ice results in melting it. Cooling the resulting water freezes it again. At a given pressure, water and ice can coexist at only one temperature. The water-ice coexistence temperature at ambient pressure is of such importance for everyday life that it serves as the zero-point of the widely used temperature scale invented by the Swedish physicist Celsius. Closer inspection of the melting and freezing transition shows that this transition is not quite symmetric. Ice heated above 0°C always melts, whereas cooling it below 0°C does not always result in immediate freezing. In fact, water and most other liquids can be cooled significantly below their freezing temperature and kept there without crystallizing (1, 2). This phenomena is known as supercooling. A supercooled liquid can be triggered into freezing by adding a little bit of the corresponding solid. A single snowflake in a glass of supercooled water will induce freezing of water that touches it and grow rapidly into a big chunk of ice. Other disturbances, such as dust or even shocks, can trigger the freezing of supercooled liquids as well. It thus seems difficult for the

freezing process to begin spontaneously, but once initiated, it perpetuates easily. The spontaneous formation of a piece of solid ice is an example of nucleation.

The fact that a liquid can be supercooled is best understood qualitatively in the framework of classical nucleation theory (CNT) (see, e.g., Reference 3). According to CNT, the free energy of a spherical nucleus that forms in a supersaturated solution contains two terms. The first term accounts for the fact that the solid phase is more stable than the liquid phase. This term is negative and proportional to the volume of the nucleus. The second term is a surface term. It describes the free energy needed to create a solid/liquid interface. This term is positive and proportional to the surface area of the nucleus. The Gibbs free energy of a spherical nucleus of radius R has the following form:

$$\Delta G = \frac{4}{3}\pi R^3 \rho_s \Delta\mu + 4\pi R^2 \gamma, \tag{1}$$

where ρ_s is the number density of the bulk solid, $\Delta\mu$ the difference in chemical potential between the solid and the liquid, and γ is the solid/liquid-surface free-energy density. The function ΔG has a maximum at $R = 2\gamma/(\rho_s|\Delta\mu|)$, and the corresponding height of the nucleation barrier is given by

$$\Delta G^* = \frac{16\pi}{3}\frac{\gamma^3}{(\rho_s|\Delta\mu|)^2}. \tag{2}$$

For small nuclei, the surface term dominates and the free energy increases. Only if this nucleus exceeds a critical size does its free energy decrease, and the crystallite can grow spontaneously. The probability for the formation of a critical nucleus depends exponentially on its free energy of formation:

$$P_c \propto \exp(-\Delta G^*/k_B T). \tag{3}$$

The crystal-nucleation rate is given by the product of P_c and a kinetic factor Γ that describes the rate at which a critical nucleus grows. The CNT expression for the nucleation rate per unit volume is

$$I = \Gamma \exp\left[-\frac{16\pi}{3k_B T}\frac{\gamma^3}{(\rho_s|\Delta\mu|)^2}\right], \tag{4}$$

where $\Gamma = Z\rho_l f_c^+$. Here, ρ_l is the number density of the liquid, $Z = \sqrt{|\Delta\mu|/6\pi k_B T n_c}$ is the Zeldovich factor, and f_c^+ is the attachment rate of particles to the critical cluster that contains n_c particles. The Zeldovich factor arises from the fact that not all particles that are at the top of the nucleation barrier crystallize: Some will recross the barrier and melt again. The attachment rate of particles to the critical nucleus can be estimated by multiplying the number of monomers available at the surface of the nucleus (which is proportional to $n_c^{2/3}$) to the typical transition rate at which these particles become part of the nucleus. This transition rate is proportional to D_S/λ^2, where D_S is a self-diffusion coefficient and λ is a

typical distance over which diffusion takes place:

$$f_c^+ = \frac{24 D_S {n_c}^{2/3}}{\lambda^2}. \quad (5)$$

The above expression for the nucleation rate is the one most commonly used to analyze crystal-nucleation rate experiments. The problem with the CNT approach is that, in most cases, neither λ nor γ are accurately known. More often than not, both parameters are obtained by fitting the CNT expression to experimental nucleation data. In fact, the situation is even more confusing as a clear microscopic definition of the "jump distance" λ is lacking, while there is considerable ambiguity in the choice of the correct microscopic expression for the surface free-energy density γ.

To illustrate the problems associated with the fitting of CNT to experimental data, we consider an example from recent experiments on crystallization in hard-sphere colloids. Palberg (4) fitted the data from Harland & van Megen (5) and obtained $\gamma = 0.5 k_B T/\sigma^2$ and $\lambda = 17 d_{NN}$, whereas for the data from Heymann et al. (6), he found $\gamma = 0.54 k_B T/\sigma^2$ and $\lambda = 2.8 d_{NN}$, where σ is the particle diameter and d_{NN} is the nearest neighbor distance. The estimates for the surface free energy are rather low when compared with numerical estimates (7), and the values of the effective jump length λ seem rather large (a factor 10 to 100 times larger than the mean free path in the liquid). However, as the experimental results could be fitted with Equation 4, there was little reason to doubt the values of the fit parameters obtained from experiment.

Because experiments to determine absolute crystal-nucleation rates are notoriously difficult, there is a clear need for a first principle prediction of a crystal-nucleation rate.

In this review, we discuss some of the recent progress that has been made in the application of computer simulation to gain a better understanding of the kinetics of colloidal crystallization. As is explained below, simulation techniques have now progressed to the point where—for the first time—it is possible to compute absolute crystal nucleation rates under conditions that correspond to those used in experiments. Moreover, we are able to study in detail the nucleation pathway. The simulations described in this review focus on colloidal crystallization. The reasons for this choice is twofold: First, the interactions between spherical colloids are thought to be well known. And second, colloidal crystallization can be studied experimentally using real-space imaging techniques. In other words, these are ideal systems to confront experiment and simulation. Interestingly, the simulations suggest that our understanding of such colloidal systems is far from complete.

2. METHOD

Simulating the crystallization process is a computational challenge, precisely because crystal nucleation is an activated process. This implies that the formation of small crystal nuclei in a supersaturated liquid is infrequent, but when it happens,

the process is quite fast, i.e., it proceeds on a timescale that can be followed in a molecular simulation. For instance, experimentally measured nucleation rates are typically on the order of $\mathcal{O}(10^1)$ to $\mathcal{O}(10^6)$ nuclei per cm^3 per sec. We can estimate the number of time steps needed in a molecular dynamics (MD) simulation to observe one nucleation event. In a large-scale computer simulation, it is feasible to study the dynamics of $\mathcal{O}(10^6)$ particles, but the number of particles in a typical simulation is some two to three orders of magnitude less. For an atomic liquid, the volume of a simulation box containing one million particles is of order $\mathcal{O}(10^{-15})\,cm^3$. If one million nuclei form per second in one cubic centimeter, then it will take, on average, 10^9 seconds for a nucleus to form in a system of one million particles. Because the typical time step in an MD simulation is on the order of femtoseconds, this implies that it would take some 10^{24} MD time steps to observe a single nucleation event under experimental conditions.

This example illustrates why it is difficult to compute nucleation rates using conventional MD simulations. One way around this problem is to simulate a system at a much higher supersaturation, where the free-energy barrier for the formation of crystal nuclei is sufficiently low to allow the system to crystallize spontaneously on a timescale that is accessible in an MD simulation. The problem with this approach is that, at such extreme supersaturations, crystallization may proceed differently than at moderate supersaturations. For example, at high supersaturations, many crystal nuclei may form simultaneously and may interact in an early stage of their development. It then becomes difficult to compare the computed crystallization rates with predictions based on CNT.

To study crystal nucleation at moderate supersaturation, we exploit the fact that the crystallization rate is determined by the product of a static term, namely the probability of the formation of a critical nucleus P_c, and a kinetic factor Γ that describes the rate at which such nuclei grow. We use umbrella sampling to compute P_c and kinetic Monte Carlo simulations to compute Γ. The computed nucleation rates can be directly compared with experimental data.

In the following, we briefly summarize the numerical techniques needed to compute a nucleation rate based on Reference 8. First we discuss the calculation of the cluster size distribution. Then we turn to the calculation of the kinetic prefactor.

2.1. Calculation of the Cluster Size Distribution

The probability that a crystal nucleus of size n will form can be approximated by $P(n) = N_n/N$, where N_n is the number of crystal nuclei of size n in a system containing N particles (8–10). The approximation becomes better as N_n/N becomes smaller, i.e., when the spontaneous formation of clusters is rare. Knowledge of the ratio N_n/N allows us to define the Gibbs free energy $\Delta G(n)$ for the formation of a nucleus of size n:

$$\frac{N_n}{N} = \exp[-\Delta G(n)/k_B T]. \tag{6}$$

Before we can calculate N_n in a Monte Carlo simulation, we need to have a numerical technique that enables us to distinguish between particles in a liquid environment and those in a solid one. To this end, we use local bond-order analysis introduced by Steinhardt et al. (11) and applied to study nucleation by Frenkel and coworkers (8, 12, 13). The advantage of this analysis is that it is sensitive only to the overall degree of crystallinity in the system, but independent of any specific crystal structure. This requirement is important as otherwise we would apply an external biasing potential that could force the system to crystallize in a specific structure. A second advantage is that these bond-order parameters can be constructed so as to be independent of the reference frame. In particular, the local bond-order parameter that we use and assign to each particle is suitable to distinguish between crystal structures that have a sixfold symmetry (i.e., the bcc, fcc, and hcp structures) and the liquid. It has the following form:

$$q_6(i) = \left(\frac{4\pi}{13} \sum_{m=-6}^{6} |q_{6m}(i)|^2 \right)^{1/2} \tag{7}$$

with

$$q_{6m}(i) = \frac{1}{N_b(i)} \sum_{j=1}^{N_b(i)} Y_{6m}(\hat{\mathbf{r}}_{ij}). \tag{8}$$

Here, the sum goes over all neighboring particles $N_b(i)$ of particle i. Neighbors are usually defined as all particles that are within a given radius r_q around a particle. $Y_{6m}(\hat{\mathbf{r}}_{ij})$ is the m-component of the spherical harmonics evaluated for the normalized direction vector $\hat{\mathbf{r}}_{ij}$ between the neighbors. The local bond-order parameters are sensitive to the degree of orientational correlations of the vectors that join neighboring particles. In simple liquids, we expect that there are no preferred orientations around a particle and therefore the correlations decay rapidly. In contrast, for a particle with a solid-like environment the vectors are correlated. Thus we expect to obtain a separation of the distribution function for the liquid and the solid by calculating the correlation function of the vectors $\mathbf{q}_6$ of neighboring particles i and j:

$$\mathbf{q}_6(i) \cdot \mathbf{q}_6(j) = \sum_{m=-6}^{6} q_{6m}(i) \cdot q_{6m}^*(j), \tag{9}$$

where the asterisk indicates the complex conjugate. We now define two neighboring particles i and j as being connected if the dot product exceeds a certain threshold. In general, this criterion is insufficient to draw a sharp distinction between liquid and solid particles. We therefore apply a second crystallinity criterion based on the number of "connections" that a particle has with its neighbors.

This analysis provides us with an unambiguous local criterion to identify solid-like particles. Finally, we need to have a criterion for identifying clusters. The criterion we applied is that if two solid-like particles are less than a certain threshold

distance apart, then they belong to the same cluster. We note that, whereas the absolute number of particles in the cluster depends somewhat on the choice of the threshold values, the height of the computed free-energy barriers is fairly insensitive to the precise criterion that is used.

Using this local bond-order analysis, we can sample the equilibrium distribution function for the probability $P(n)$ in a Monte Carlo simulation. In all cases, we performed Monte Carlo simulations in the isobaric-isothermal (NPT) ensemble. In this ensemble, the average of a microscopic quantity A is given by

$$\langle A \rangle_{NPT} = \frac{\int dV \int d\mathbf{r}^N A(\mathbf{r}^N) \exp[-\beta(U(\mathbf{r}^N) + PV)]}{\int dV \int d\mathbf{r}^N \exp[-\beta(U(\mathbf{r}^N) + PV)]}, \tag{10}$$

where $U(\mathbf{r}^N)$ is the potential energy of the system with particle positions $\mathbf{r}^N$, $\beta = 1/k_BT$ is the reciprocal of the thermal energy, N the number of particles, and P the applied pressure. Because the formation of crystal nuclei containing more than ten particles is very rare, we sampled the formation of such clusters using biased sampling (14). The method is based on the idea that the ensemble average can be rewritten as follows:

$$\langle A \rangle_{NPT} = \frac{\langle A/W(\mathbf{r}^N) \rangle_W}{\langle W(\mathbf{r}^N)^{-1} \rangle_W}, \tag{11}$$

where we have introduced an as-yet-unspecified weighting function $W(\mathbf{r}^N) = \exp[-\beta\omega(\mathbf{r}^N)]$, where $\omega(\mathbf{r}^N)$ is the biasing potential. The subscript $\langle \ldots \rangle_W$ indicates an ensemble average according to the biased distribution function $\exp[-\beta(U(\mathbf{r}^N) + PV)]W(\mathbf{r}^N)$. By specifying the weighting function W, we can force the system to sample in the relevant regions of phase space.

Because the formation of large nuclei is rare, the probability that two large clusters will exist simultaneously in the system is extremely small. As a consequence, we can choose a bias potential that controls just the size of the largest cluster in the system. Somewhat arbitrarily, we chose the bias potential to be a harmonic function of the size of the largest cluster:

$$\omega[n(\mathbf{r}^N)] = \frac{1}{2}k_n[n(\mathbf{r}^N) - n_0]^2. \tag{12}$$

The constant k_n determines the range of cluster sizes sampled in one simulation. The parameter n_0 determines the center of the "window." In principle, we should be able to design a biasing function that makes it possible to sample all cluster sizes in a single simulation. However, such a "smart" simulation would take much longer to equilibrate (15). This is why we split the simulation into a number of smaller simulations that are restricted to narrow, but overlapping, windows of different cluster sizes. The implementation of the biasing potential in the Monte Carlo simulation is straightforward. Because the computation of cluster sizes is relatively time consuming, we do not compute the size of the largest cluster after every Monte Carlo move. Rather, we carry out a fixed number of Monte Carlo moves per particle without bias. We then calculate the final cluster size and accept

or reject the whole sequence of trial moves on the basis of the change in the biasing potential: $\exp[-\beta\Delta\omega]$, where $\Delta\omega$ is the difference in the biasing potential after and before the trajectory. To facilitate the (very slow) stacking rearrangements of the clusters, we implemented the parallel tempering scheme of Geyer & Thompson (16). The idea is to run all the simulations in the different windows in parallel and allow them to exchange clusters between adjacent windows. The actual change between windows i, j is accepted according to $\exp[-\beta(w_n - w_o)]$, where $w_o = k_i/2(n_i - n_{0,i})^2 + k_j/2(n_j - n_{0,j})^2$ is the energy of the biasing potential before and $w_n = k_i/2(n_j - n_{0,i})^2 + k_j/2(n_i - n_{0,j})^2$ after the change. In practice, what is exchanged between processors are the minima of the bias potential rather than the configurations. This requires virtually no communication between different computer nodes. The Gibbs free energies of the systems in the different windows are determined up to a constant $\Delta G_i(n)/k_BT + b_i$, where the subscript i indicates the number of the window. To determine the constant b_i, we fitted all the free-energy estimates in the different windows to one polynomial in n. This can be done by a linear least-squares fit, where we minimize

$$\chi = \sum_{n=1}^{n_{max}} \left\{ \sum_{i=1}^{n_w} w_i(n) \left[\Delta G_i(n) - \sum_{k=1}^{k_{max}} a_k n^k - b_i \right]^2 \right\}. \qquad (13)$$

Here, $w_i(n) = 1/\sigma^2_{\Delta G_i(n)}$ is the statistical weight determined by the variance $\sigma^2_{\Delta G_i(n)}$ of the free-energy measurement, and n_w is the total number of windows used in the simulation. The total number of cluster sizes considered is denoted by n_{max} and k_{max} fixes the order of the polynomial fit.

2.2. Kinetic Prefactor

In atomistic simulations, the kinetic prefactor is usually calculated using the Bennett-Chandler scheme (17). This scheme was originally devised to study activated processes in simple molecular systems. In such systems, barrier crossings are often almost ballistic, i.e., a system that crosses the top of the free-energy barrier in the forward direction will, with high probability, continue to form the reaction products. However, in systems where the motion over the barrier is strongly damped (e.g., owing to viscous friction), the motion over the free-energy barrier is diffusive: The probability that a system that crosses the top of the barrier in the forward direction will end up on the product side, is barely larger than 50%.

When the barrier crossing is relatively diffusive, it is attractive to use a modification proposed by Ruiz-Montero et al. (18). The principle of both methods is to generate a large number of independent configurations at the top of the barrier. These configurations are then used as the starting point for an unbiased trajectory in which one determines if the nucleus grows and the system crystallizes, or if the nucleus shrinks. From the number of nuclei that grow and shrink one can extract the kinetic factor. However, to get a reasonable estimate, one has to simulate a rather large number of trajectories, on the order of 100.

Here, we consider barrier-crossing phenomena that are, effectively, purely diffusive. In this case, we can compute the kinetic prefactor directly using the expression $\Gamma = Z\rho_l f_{n_c}^+$. After a barrier calculation at number density ρ_l, the only unknown quantity is $f_{n_c}^+$. To compute $f_{n_c}^+$, we assume that the critical cluster grows and shrinks via the diffusive attachment of single particles. We can then define an effective diffusion constant for the change in critical cluster size:

$$D_{n_c}^{att} = \frac{1}{2}\frac{\langle \Delta n_c^2(t)\rangle}{t}, \tag{14}$$

where $\Delta n_{n_c}^2(t) = [n_c(t) - n_c(t=0)]^2$ is the mean square change in the number of particles in the critical cluster. Because the slope of this change is related to the corresponding attachment rates via $\langle \Delta n_c^2(t)\rangle/t = (f_{n_c}^+ + f_{n_c}^-)/2$, and at the top of the barrier, the forward and backward rates are equal ($f_{n_c}^+ = f_{n_c}^-$), we get

$$f_{n_c}^+ = \frac{1}{2}\frac{\langle \Delta n_c^2(t)\rangle}{t}. \tag{15}$$

This is a general expression for the calculation of the kinetic factor for diffusive barrier crossing. Using an MD simulation, one only needs to measure the change in size of the critical cluster as a function of time. The only restriction is that during the measurement the critical nucleus needs to fluctuate around its critical value. To apply this method for the calculation of the attachment rate in a colloidal suspension, we need to have a simulation technique that generates trajectories following Brownian dynamics, and hydrodynamic interaction also needs to be considered. Trajectories following Brownian dynamics can be generated using a kinetic Monte Carlo scheme proposed by Chichocki & Hinsen (19). To correct for the effect of hydrodynamic interactions that are known to be important at high-volume fractions, we used an approach proposed by Medina-Noyola (20). We replaced the free-diffusion coefficient D_0 by the short-time self-diffusion coefficient D_S^S. We therefore have to multiply our result by a factor $\alpha = D_S^S/D_0$. For hard spheres, several (rather similar) functional forms for this factor have been proposed (21–24). Here, we used the phenomenological expression $(1 - \phi/0.64)^{1.17}$ (25) at high-volume fraction ϕ. To test our approach, we computed the long-time self-diffusion coefficient of a dense colloidal suspension of hard spheres. The present method reproduces the experimental data to within the statistical error (8).

3. HARD-SPHERE COLLOIDS

A collection of hard identical spheres is the simplest possible model system that undergoes a first-order phase transition. For low-packing fractions, the particles are in a liquid state, but when the packing fractions exceed a value of 49.4%, an ordered solid state becomes more stable. This was first shown in computer simulations by Hoover & Ree (26) in 1968. The experimental realization of a colloidal suspension that closely mimics the phase behavior of hard spheres followed approximately 20 years later and was a milestone in soft-matter physics

(27, 28). More recently, the phase-transition kinetics of hard-sphere colloids has been studied extensively in experiments (5, 29, 30). However, as mentioned in the introduction, the interpretation of the data with CNT was rather indirect.

Using the simulation techniques described above, we can compute the rate of crystal nucleation for hard-sphere colloids by a direct calculation of the nucleation barrier and the kinetic prefactor (8, 31). We first performed Monte Carlo simulations in the isobaric-isothermal ensemble *NPT* to compute the crystal-nucleation barrier at three different pressures, $\beta P\sigma^3 = 15, 16$, and 17. The corresponding bulk volume fractions of the liquid are $\phi = 0.5207, 0.5277$, and 0.5343. The resulting nucleation barriers are shown in Figure 1. As expected, with increasing volume fraction, the crystal-nucleation barrier decreases. Our simulation results for the crystal-nucleation barrier can be compared directly to the predictions from CNT for the nucleation barrier (Equation 1). For the hard-sphere system, the chemical potential difference can be calculated accurately using phenomenological equations of state for the liquid and the solid (32). Because the solid-liquid interfacial free-energy γ of a small crystal nucleus in a supersaturated liquid is not known a priori we use its corresponding value for a flat interface at coexistence. This value has been calculated in a recent simulation (7) for three different crystal planes. Here we use $\gamma_{av} = 0.61 k_B T/\sigma^2$, which is the average of the three crystal planes. The results for the barrier height based on CNT in order of increasing density are $\Delta G^*/k_B T = 27, 15.7$, and 10.2. These values are approximately 30–50% lower than our numerical estimate. This discrepancy might be due to the fact that for a small nucleus in a supersaturated liquid the interfacial free energy is different from that of a flat interface at coexistence. For this reason, we also used γ as a fit parameter to our results. Using $R = (3n/(4\pi\rho_S))^{1/3}$, we fitted Equation 1 to our data. The result can be seen as the solid line in Figure 1. The functional form of the nucleation barrier seems to be described well by CNT, but the values for the fit parameter $\gamma_{eff}(P = 15) = 0.71 k_B T/\sigma^2$, $\gamma_{eff}(P = 16) = 0.737 k_B T/\sigma^2$, and $\gamma_{eff}(P = 17) = 0.751 k_B T/\sigma^2$ are higher than the coexistence value and they increase with volume fraction. If we assume that this dependence is linear, then our simulation results extrapolate to a value of $\gamma_{eff}(P = 11.7) = 0.64 k_B T/\sigma^2$ at coexistence—a value that is very close to γ_{av}. For a discussion of the dependence of the surface free-energy density on supersaturation, see Reference 33.

Our results for the surface free-energy density can also be compared with the values extracted from experiments. Palberg (4) fitted the data from Harland & van Megen (5) and obtained $\gamma = 0.5 k_B T/\sigma^2$, and for the data from Heymann et al. (6), he found $\gamma = 0.54 k_B T/\sigma^2$. These values are significantly lower than the numerical estimates.

In the crystal-nucleation experiments, the colloids had a size polydispersity of approximately 5%. We therefore repeated our simulations for a suspension with 5% polydispersity. We found that both systems have the same nucleation barrier at the same $\Delta\mu$ (34). Therefore, polydispersity alone cannot account for the difference between the barrier heights derived from experiment and those derived from simulation.

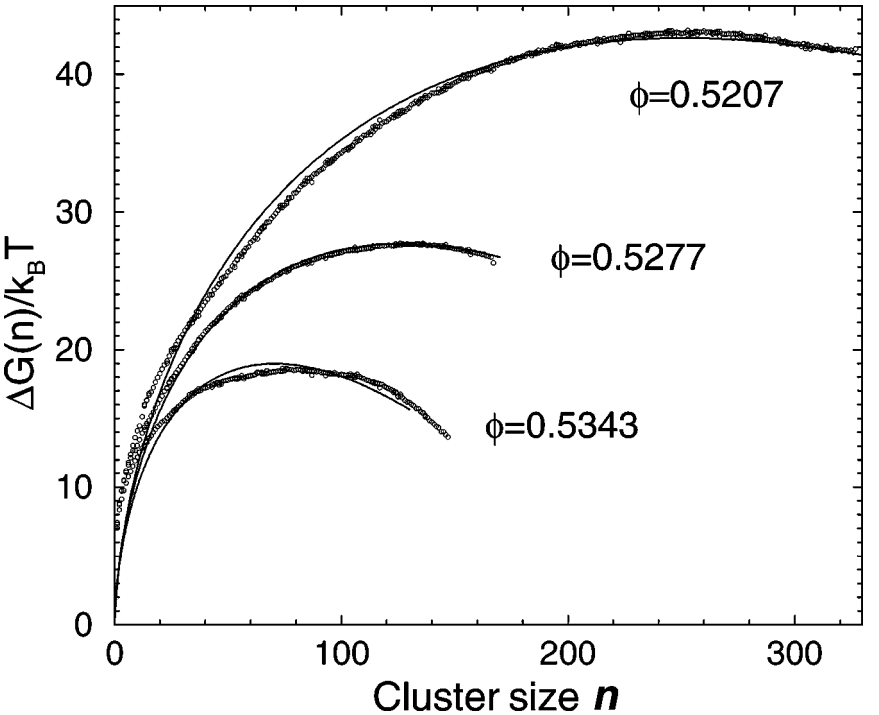

Figure 1 Calculated free-energy barrier for homogeneous crystal nucleation of hard-sphere colloids. The results are shown for three values of the volume fraction. The drawn curves are fits to the CNT expression (Equation 1). For the identification of solid-like particles, we used the techniques described in the text (see Section 3). The cutoff for the local environment was set to $r_q = 1.4\sigma$, the threshold for the dot product $q_6 q_6 = 20$, and the threshold for the number of connections was set to 6. If two solid-like particles are less than 2σ apart, where σ is the diameter of a particle, then they are counted as belonging to the same cluster. The total simulation was split up into a number of smaller simulations that were restricted to a sequence of narrow, but overlapping, windows of n values. The minimum of the bias potential was placed in steps of tens, i.e., $n_0 = 10, 20, 30,$ etc. In addition, we applied the parallel tempering scheme of Geyer & Thompson (16) to exchange clusters between adjacent windows. All simulations were carried out at constant pressure and with the total number of particles (solid plus liquid) fixed. For every window, the simulations took at least 1×10^6 MC moves per particle, excluding equilibration. To eliminate noticeable finite-sized effects, we simulated systems containing 3375 hard spheres. We also used a combined Verlet and Cell list to speed up the simulations.

TABLE 1 Summary of the simulation results for the calculation of the nucleation rate for monodisperse hard-sphere colloids.

ϕ	ΔG^*	n_c	f_c^+/D_0	$\mathbf{Log_{10}}[I^*]$	λ	$\Delta\mu$
0.5207	43.0	260	189	−19.3	0.31	0.34
0.5277	27.8	130	43	−13.5	0.46	0.44
0.5342	18.5	75	66	−9.14	0.27	0.54

Here, ϕ is the volume fraction of the liquid phase. ΔG^* is the measured free energy to form a cluster of critical size n_c. f_c^+/D_0 is the attachment rate of particles to the critical cluster divided by the free-diffusion coefficient. $I^* = I\sigma^5/D_0$ is the reduced nucleation rate, and λ is the estimated typical jump distance from the calculation of the attachment rate. $\Delta\mu$ is the difference in chemical potential between the two phases.

Subsequently, we performed kinetic Monte Carlo simulations to compute the kinetic prefactor and, thereby, the absolute crystal nucleation rate. The results of our calculations of the attachment rate for the monodisperse hard-sphere system are summarized in Table 1. Because experimentally determined values for the kinetic factor often differ by orders of magnitude from those predicted by CNT, it is also important to compare our computed kinetic prefactor with the one predicted by CNT. We found that the Zeldovich factor that follows from our numerical calculations is almost identical to the CNT prediction. This is not surprising, as CNT provides a good fit to the numerical data for the shape of the barrier. The remaining quantity to compare is the reduced attachment rate f_c^+/D_0. If we assume that in Equation 5 $D_S = D_S^L$, where D_S^L is the long-time self-diffusion constant, and if we treat λ as a fit parameter to reproduce our calculated attachment rates, then we get values for λ in the range 0.27–0.46σ (see Table 1). This jump distance—in the case of colloids it might be better to call it a diffusion distance— is comparable to the interparticle spacing in a dense suspension, which seems reasonable. In contrast, experimental estimates for λ tend to be unrealistically large: $\lambda = 2.8$–17σ (4). The identification $D_S = D_S^L$ is justified by the fact that the time λ^2/D_S^L corresponds to long-time diffusion.

Using simulation results, we can compute steady-state nucleation rates that can be compared directly (i.e., without any adjustable parameters) to experiment. In Figure 2, we show our numerical predictions for the nucleation rate of a monodisperse suspension and a suspension with 5% polydispersity. These results can be compared directly to the experiments on suspensions with the same polydispersity. In Reference 30, the polydiversity is approximately 2.5%. As shown in Figure 2, the simulations predict a much stronger dependence of the nucleation rates on density than is observed in the experiments. This discrepancy between the simulations and experiment is unexpected and significant because hard-sphere colloids are among the best-studied experimental realizations of a simple liquid. We know the structural and thermodynamic properties of hard-sphere suspensions quite accurately, and more significantly, these properties tend to be well reproduced by the ideal hard-sphere model. Hence, large discrepancies between experiment and simulation cannot be easily dismissed as due to uncertainties in the parameters that

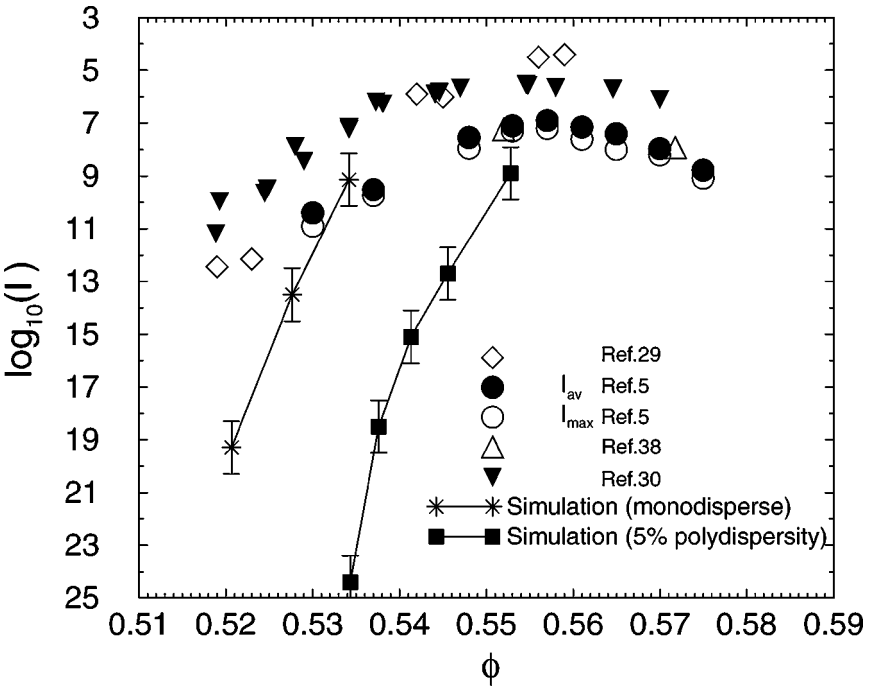

Figure 2 Reduced nucleation rates ($I^* = I\sigma^5/D_0$) as a function of the volume fraction of the metastable liquid. The simulation data for monodisperse colloids are indicated by the ∗–∗, the drawn curve joining the simulation points is meant as a guide to the eye. In the same figure, we show the experimental results of Reference 29 (◇), Reference 5 (○ and ●), Reference 38 (△), and Reference 30 (▼). We also performed simulations on model systems that have the same polydispersity (5%) as the experimental systems. These simulation results are denoted by the filled squares.

characterize the colloidal suspension. Rather, we must first envision the possibility that either our theoretical description of crystallization is inadequate or that what is measured is not really the steady-state, homogeneous nucleation rate. In fact, the latter suggestion is not altogether unreasonable, as light-scattering cannot be used to see the very early stages of crystal nucleation. Second, the experiments are extremely sensitive to any residual ordering in the solution that may have survived the preparation of the experimental system. Third, at high supersaturations, the concentration of crystal nuclei rapidly becomes sufficiently large such that the interaction between different crystal nuclei may no longer be ignored (35). In that case, the steady-state nucleation expressions that we employ are no longer applicable. Dixit & Zukoski (36) developed a purely kinetic model to predict nucleation rates that yields good quantitative agreement with the experimental

data. Volkov et al. (37) recently reported molecular dynamic simulations of hard-sphere crystallization at large supersaturations. In this regime, the simulations are in good agreement with experiment. In fact, in the simulations by Volkov et al. (37), the simulation data were analyzed in the same way as the experiments (namely, by studying the time evolution of the first Bragg peak of the static structure).

A unique feature of the simulations is that they allow us to study in detail the structure of small crystal nuclei. This is interesting given that Ostwald (39) had already described the role of metastable phases in crystal nucleation when he formulated his famous step rule in 1897. This rule states that the phase that nucleates does not need to be the one that is thermodynamically most stable. In recent years, there have been several attempts to provide a microscopic explanation for Ostwald's observation (40–43). Alexander & McTague (40) argue, on the basis of Landau theory, that if the differences in the liquid and solid densities were not too great, then the phase that was nucleated from the liquid would be bcc regardless of the structure of the stable (lowest free-energy) phase. Klein & Leyvraz (41, 42) showed that for deeply quenched systems with long-range interactions, the critical droplet can have a bcc symmetry, but not a bcc crystalline structure. Simulations by ten Wolde et al. (13) showed that the situation can be even more subtle, at least for a Lennard-Jones system: The core of a stable Lennard-Jones cluster formed a stable fcc structure, whereas the surface of the nucleus showed indications of a bcc structure. Thermodynamically, the formation of metastable phases might be explained by differences in interfacial free energies. The formation of a bcc-liquid interface might cost less energy than that of a fcc-liquid interface. For hard spheres, it is known that the fcc phase is the stable structure, but the free-energy difference between the fcc and the hcp structure is very small ($<10^{-3}k_BT$) (44, 45). This means that thermal fluctuations of the order of k_BT could transform a cluster of 1000 particles from fcc to hcp or just cause stacking faults. The fcc and the hcp structures differ only in the stacking of close-packed hexagonal crystal planes. For the fcc structure, the stacking is ABC, whereas for the hcp structure, the stacking is AB. If the interfacial free energies of a crystal fcc-liquid, hcp-liquid, or an rhcp-liquid interface are different, then this picture could completely change. Here, rhcp refers to a random stacking of the close-packed hexagonal crystal planes. Whether small crystal nuclei are more like fcc or hcp is not clear. Experiments by Pusey et al. (46) and Haddon et al. (47) indicate that the fcc structure is favored. However, microgravity experiments by Zhu et al. (48) showed that, initially, small crystal nuclei have an rhcp structure. A snapshot of the cross section of a simulated critical nucleus is shown in Figure 3. From a direct inspection of the nuclei, we found that the structure of the nuclei is rhcp. To carry out the stacking analysis, the nuclei needed to have a size of at least 150 particles, otherwise the number of layers is too small to distinguish in a meaningful way between different stackings. To study the structure of even smaller nuclei, we performed a local bond-order analysis. This analysis also suggests that the rhcp structure is dominant. This was also found in more recent simulations by O'Malley

& Snook (49). Surprisingly, these simulations also showed evidence for multiply twinned nuclei with a decahedral morphology.

4. EFFECT OF POLYDISPERSITY

In practice, the colloidal particles used in the experiments have a distribution of particle radii (referred to as polydispersity) that is rarely less than 2–3% of the average radius. To compare our measured nucleation rates with experiments, we studied the effect of a small polydispersity (up to 5%) (as described in the preceding sections). For polydispersities up to 5%, we found no effect of polydispersity on the height of the nucleation barrier. However, experiments on hard-sphere colloids indicate that crystallization is suppressed if the polydispersity exceeds 12% (50). This suppression of crystallization is usually attributed to the fact that in polydisperse suspensions the freezing point is shifted to higher densities where the system tends to become glassy. In a glass, the kinetic prefactor Γ is expected to be very small, but the nucleation barrier should continue to decrease with increasing supersaturation. To test this, we studied the behavior of the crystal-nucleation barrier for polydispersities up to 10% (34). We performed Monte Carlo simulations in a constant-pressure, semigrand-canonical ensemble (as described in Reference 51). In these simulations, we computed the crystal-nucleation barrier and the structure of the critical nucleus as a function of both polydispersity and supersaturation. As with monodisperse suspensions (31), we found that all critical nuclei had a randomly stacked close-packed structure. During crystallization, size-fractionation occurs (51, 52): The particles that make up the critical nucleus are, on average, larger than those in the metastable liquid. We found that ΔG^*, the height of the nucleation barrier, at fixed $|\Delta\mu|$ does not depend on the polydispersity for polydispersities $\leq$5% (see Figure 4). However, as the polydispersity is increased beyond 5%, ΔG^* increases rapidly. This implies that the probability that a critical nucleus forms is suppressed in polydisperse suspensions. It follows from Equation 2 [or actually from its polydisperse equivalent (see Reference 8)] that at constant $|\Delta\mu|$, the variation of ΔG^* with polydispersity is due to an increase of the interfacial free-energy γ. The increase of γ with polydispersity runs counter to Turnbull's suggestion that the interfacial free energy should be proportional to ΔH, the latent heat of fusion (3). For the systems that we studied, ΔH crosses zero at a polydispersity of 9% (53), where the liquid becomes denser than the coexisting solid (51). Yet, γ clearly remains nonzero.

Surprisingly, the variation of ΔG^* with $|\Delta\mu|$ is nonmonotonic. As $|\Delta\mu|$ is increased, the nucleation barrier goes through a minimum (Figure 4). This nonmonotonic behavior of ΔG^* is due to the increase of γ with $|\Delta\mu|$. To illustrate this, let us approximate the $|\Delta\mu|$ dependence of γ by $\gamma \approx \gamma_0(1+a|\Delta\mu|)$. Ignoring the slight $|\Delta\mu|$ dependence of the solid density, it then follows from Equation 2 that ΔG^* must go through a minimum when $|\Delta\mu| = 2/a$. The nucleation theorem (54–56) suggests that the minimum in ΔG^* is due to the

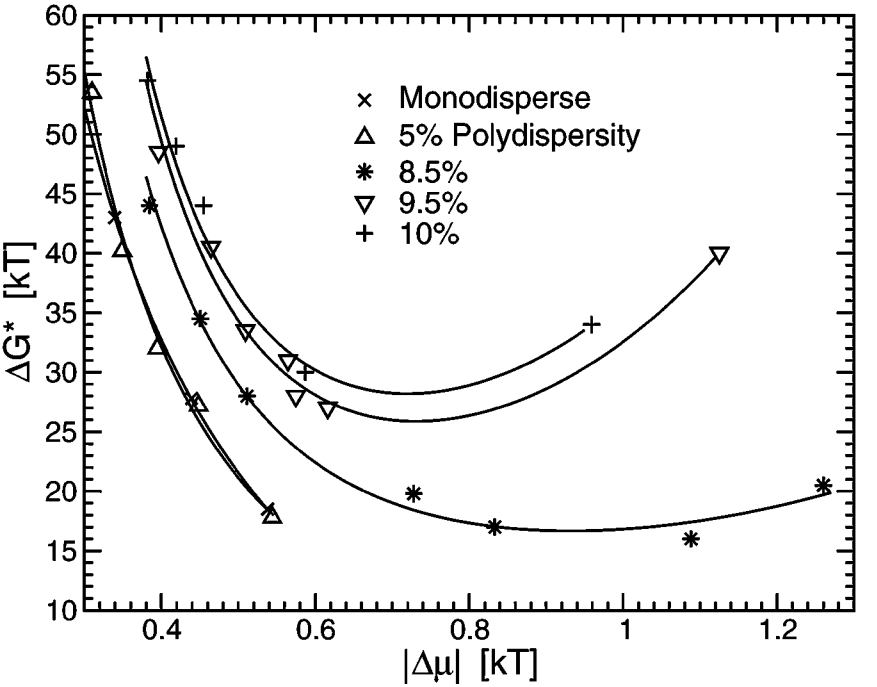

Figure 4 Computed dependence of the free-energy barrier for crystal nucleation of polydisperse suspensions of hard, colloidal spheres. The free energy is expressed in terms of k_BT, where k_B is Boltzmann's constant and T is the absolute temperature. $|\Delta\mu|$ (also in units of k_BT) is the absolute difference between the chemical potential of the liquid and the solid. It is a measure of the degree of supersaturation. The curves are fits that have been drawn as a guide to the eye. In Table 2 we have collected the data on the relation between $|\Delta\mu|$ and the volume fraction ϕ of the liquid for the different systems that we studied, to facilitate comparison with experiment.

inversion of the densities of the polydisperse fluid and the crystal nucleus. In CNT it is usually assumed that γ is constant. A linear variation of γ with $|\Delta\mu|$ has been observed in inorganic glasses (3), but there the constant a is negative and hence there is no minimum in ΔG^*. In other systems (57, 58), nonmonotonic behavior of ΔG^* is induced by a hidden phase transition in the metastable phase.

The minimum value of ΔG^* increases rapidly with polydispersity. Using kinetic Monte Carlo simulations, we can estimate the value of the kinetic prefactor (19). We find that, over the range of supersaturations studied, the kinetic prefactors vary by, at most, one order of magnitude (53). This means that the variation in the rate of nucleation is dominated by the behavior of ΔG^*. We estimate that, for colloidal particles with a radius $\geq$500 nm, homogeneous nucleation will be effectively

TABLE 2 Supersaturation and volume fraction of polydisperse colloids.

0%		5%		8.5%		9.5%		10%	
$\Delta\mu$	ϕ	$\Delta\mu$	ϕ	$\Delta\mu$	ϕ	$\Delta\mu$	ϕ	$\Delta\mu$	ϕ
0.339	0.5207	0.310	0.5344	0.385	0.5614	0.397	0.5697	0.382	0.5717
0.439	0.5277	0.349	0.5377	0.451	0.5673	0.465	0.5746	0.419	0.5738
0.538	0.5342	0.395	0.5414	0.512	0.5726	0.509	0.5782	0.455	0.5775
		0.448	0.5456	0.728	0.5864	0.565	0.5808	0.587	0.5878
		0.544	0.5528	0.833	0.5948	0.575	0.5828	0.959	0.6239
				1.088	0.6145	0.616	0.5859		
				1.260	0.6212	1.125	0.6239		

$\Delta\mu$ is the supersaturation, and ϕ is the volume fraction of the colloidal fluid. For a calculation of $\Delta\mu$ in polydisperse systems (see Reference 8). The polydispersity ranges from 0% (*left*) to 10% (*right*). The polydispersities quoted in this table and in the figures, are those of the metastable liquid.

suppressed (less than one nucleus per cm^3 per day) when the polydispersity exceeds 10%. This finding has important implications for the morphology of polycrystalline colloidal materials. Using a simplified version of the analysis proposed by Shi et al. (57) to estimate the size of crystallites in a polycrystalline sample, it is easy to derive that the average crystallite size at the end of a nucleation experiment should scale as $\exp(\Delta G^*/4k_BT)$. Our observation of a minimum in ΔG^* thus implies the existence of a minimum in the typical crystallite size. This should be experimentally observable.

We can only compute ΔG^* if spontaneous nucleation does not occur in the course of a simulation. In practice, this implies that we can not study barriers lower than $15k_BT$. As a result, we cannot test whether ΔG^* in systems with a low polydispersity (less than 8.5%) also has a minimum. If we assume that we can extrapolate the increase of γ with $|\Delta\mu|$ to large supersaturations at lower polydispersities, then we predict that a minimum in ΔG^* should occur even in nearly monodisperse systems. Again, this should be experimentally observable because we should see the formation of larger crystallites if the solution is compressed rapidly through the region where ΔG^* is small.

There are two ways to interpret the experimental finding that crystallization is not observed in suspensions with a polydispersity $>12\%$: Either crystals do not form, or they are too small to be observed. Our simulations support the first interpretation. Using the approach by Shi and colleagues (57), we can estimate the maximum number of crystallites per unit volume. For a suspension of colloids with a 500-nm radius, we expect to see less than one crystallite per cubic centimeter, once $\Delta G^* > 32k_BT$. In other words, under those conditions, the colloidal glass is truly amorphous.

Our predictions concerning the structure and free energy of colloidal crystal nuclei can be tested experimentally. Recently, the technique of confocal scanning

laser microscopy was applied by Gasser et al. (59) to study the structure and size of critical crystal nuclei in dense colloidal suspensions. This technique is perfectly suited to test our predictions. Our prediction concerning the minimum in ΔG^* is even easier to verify. By visual inspection, one can verify whether the crystallites that nucleate in strongly supersaturated solutions are larger than those that form at lower supersaturations. More than a decade ago, Pusey & van Megen (28) published beautiful images of the morphology of polycrystalline hard-sphere colloids. [Similar morphologies have recently been observed in a study of colloidal crystallization in microgravity (Z.D. Cheng, W.B. Russel & P. M. Chaikin, unpublished data)]. Pusey & van Megen (28) observed an increase of the crystallite size at large supersaturations. However, they attributed this effect to heterogeneous nucleation. Hence, a direct test of our prediction is still lacking.

5. WEAKLY CHARGED COLLOIDS

Experiments on colloidal crystallization consistently show that it is much easier to crystallize charged colloids than uncharged "hard-sphere" colloids. Clearly, long-ranged repulsion has a large effect on the crystal-nucleation rate. This may even be true for colloidal suspensions of particles that are only weakly charged. Using simulations, it is possible to study in detail how repulsive interparticle forces affect the crystal-nucleation process (60).

We modeled the interaction between the charged colloids with a repulsive hard-core Yukawa potential:

$$U(r) = \begin{cases} \infty & \text{for r} < \sigma \\ \beta\epsilon \frac{\exp(-\kappa(r/\sigma - 1))}{r/\sigma} & \text{for r} > \sigma . \end{cases} \quad (16)$$

Here, κ is the inverse-screening length in units of the hard-sphere diameter σ and $\beta\epsilon$ is the value of the Yukawa repulsion at contact. β is a measure of the inverse temperature ($\beta = 1/k_B T$), where k_B is the Boltzmann constant.

The hard-core Yukawa potential phase behavior has been mapped in detail by numerical simulation (61). The computed phase diagram of Azhar et al. (61) shows a fluid-solid (bcc/fcc) and a solid-solid (bcc/fcc) coexistence line, and the diagram exhibits two fluid (bcc/fcc) triple points. The main difference between the phase diagram of the hard-core Yukawa model and that of the pure (i.e., point-particle) Yukawa potential (62) is the presence of the second triple point. This triple point sets a lower limit for the strength of the Yukawa interaction for which a bcc phase exists.

Only a few nucleation experiments on charged colloidal suspensions have been reported. Some of these were based on light-scattering studies (63, 64). More recently, Gasser et al. (59) reported a confocal microscopy study of homogeneous crystal nucleation in slightly charged hard-sphere colloids. Recent light-scattering experiments of crystallization in more highly charged colloids has been reported by Schöpe & Palberg (65) and Wette et al. (66).

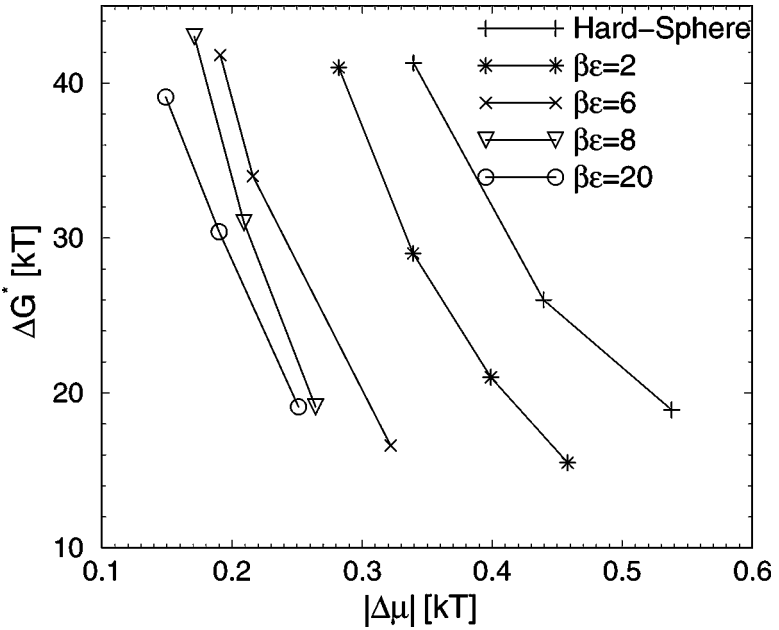

Figure 5 Calculated barrier heights of the hard-core Yukawa system with $\kappa = 5$ and $\beta\epsilon = 2, 6, 8, 20$ plotted as a function of supersaturation $\Delta\mu$ of the liquid phase to the stable fcc phase.

We performed a computer-simulation study of crystal nucleation in a hard-core Yukawa system varying both the amplitude of the Yukawa repulsion and the magnitude of the screening length. First, we computed the nucleation barrier at fixed $\kappa = 5$ for four different values of the amplitude of the Yukawa repulsion: $\beta\epsilon = 2, 6, 8$, and 20 (the results are shown in Figure 5). We found that the charge has a strong direct effect on the nucleation barrier by lowering γ. This effect is strongest when only a weak charge is added. Furthermore, we found that the functional dependence of the barrier height as a function of supersaturation does not change significantly for different charges. This is in contrast to the experiment where only a slight dependence of the nucleation rate on supersaturation was observed. In addition, we found that at the same volume fraction the nucleation barrier is much lower for weakly charged spheres than it is for hard spheres. This is partly because the fluid-solid coexistence of the charged spheres occurred at lower volume fractions, which implies a higher supersaturation. We also computed the height of the crystallization barrier for $\kappa = 10$, 5, and 3.333 at a fixed contact value, $\beta\epsilon = 8$. The effect of the range of the repulsive potential on the nucleation barrier was qualitatively similar.

Using the techniques described above, we computed the kinetic prefactors. We found that the kinetic prefactors did not vary strongly with either supersaturation or

interaction potential. Therefore, the behavior of the nucleation rate is reflected by that of the barrier height. It is interesting to compare the computed crystallization rates with the results of the confocal microscopy experiments of Gasser et al. (59). To do this, we need to know the potential parameters that best characterize the experimental system they used. Because the suspensions studied by Gasser et al. froze at a volume fraction $\phi = 0.38$, we know it is clear that the colloidal particles used in those experiments were slightly charged. It is therefore natural to describe them by a Yukawa model with a freezing point at $\phi = 0.38$. However, this condition is not sufficient to fix the values of both κ and ε. For instance, if $\kappa = 5$, then the observed freezing density can be reproduced by choosing $\beta\epsilon \sim 7$. Conversely, if $\beta\epsilon = 8$, then there are two values of κ that will reproduce the observed freezing density ($\kappa \sim 20$ and $\kappa \sim 6$) (61). In Figure 6, we show a comparison of the reduced nucleation rates reported by Gasser et al. (59) with the simulation results for those κ-$\beta\epsilon$ combinations that yield a freezing point near $\phi = 0.38$. The figure shows that different κ-$\beta\epsilon$ combinations yield very different nucleation rates. However, slopes of the different curves are all similar. Thus the main effect of varying κ and ε is to shift the nucleation curves horizontally. Comparison of the computed nucleation rates with the experimental data yields two observations: First, the experimental rates tend to be much higher than the computed rates [Gasser et al. (59) found $-6.9 \leq \log[I^*] \leq -6.5$ for volume fractions between 45% and 53%]. Second, and more important, the experiments suggest that the nucleation rate barely varies

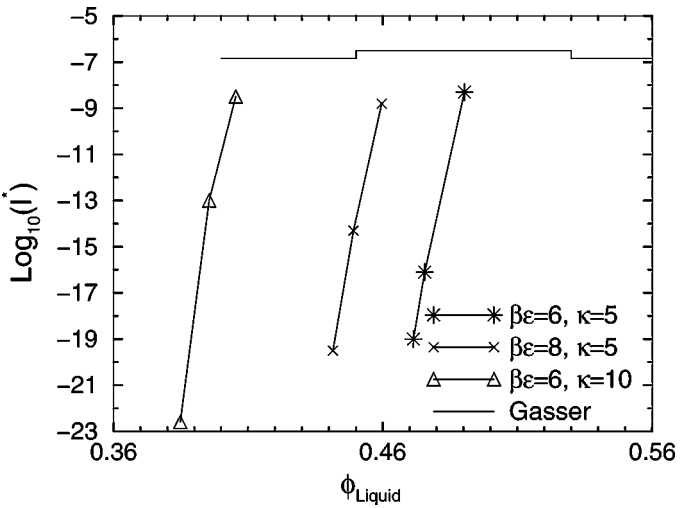

Figure 6 Comparison between the experimentally measured nucleation rates (59) and the simulation data. The nucleation rates are expressed in reduced units $I^* = I\sigma^5/D_0$, where σ is the hard-core diameter and D_0 is the self-diffusion coefficient at infinite dilution. In the plot, we added only the data sets that match the freezing density of the experimental system.

with volume fraction. We were unable to reproduce this behavior with any of the Yukawa models that we studied.

This discrepancy between experiment and simulation suggests that the experimental system is not well described by a Yukawa model with density-independent κ and ε. Conversely, it is likely that the effective potential parameters of weakly charged colloids, in the absence of added salt, depend strongly on concentration. Recent experiments by Schöpe (67) clearly illustrated this effect: With increasing concentration, the effective potential of charged polystyrene spheres in dilute aqueous solution became increasingly hard-sphere-like. If the same phenomenon occurs in more concentrated suspensions (59), then experimental results of the nucleation rates at different densities should be compared with the numerical predictions that correspond to different effective Yukawa potentials. Figure 6 shows that the variation of the nucleation rate with density can be strongly reduced (and may even become nonmonotonic) if, as we expect, ε and κ decrease with density. However, whether this effect is large enough to account for the apparent discrepancy between experiment and simulation is not clear. A truly quantitative comparison between simulation and experiment requires better knowledge of the density dependence of the effective interaction between slightly charged colloidal spheres.

The repulsive Yukawa system offers a unique opportunity to study the effect of metastable crystal phases on the pathway for crystal nucleation. To study the effect of metastable intermediates on crystallization, we analyzed the structure of the precritical nucleus in different regions of the phase diagram. The pressure range region where the bcc phase is stable is rather narrow. For these pressures, the supersaturation of the fluid phase is small; therefore, the nucleation barrier is very high. As a consequence, we can only study the formation of precritical nuclei in the fcc regime. To study the structure of the precritical nuclei, we used the local bond-order analysis proposed by ten Wolde et al. (13). In their analysis, the local bond-order signature of a nucleus is decomposed into the signatures of the different bulk structures (liquid, fcc, and bcc) using a linear least-squares fit. The value of the resulting coefficients $\{f_{liq}, f_{fcc}, \text{and } f_{fcc}\}$ are a measure of the structure of the nucleus. Our simulations showed that the precritical nuclei always have a strong bcc signature. Only for larger postcritical nuclei well within the fcc regime did we find a mixture of bcc and fcc signatures. In this sense, our simulations unambiguously support the prediction that nucleation into bcc nuclei is always uniquely favored, even when the fcc phase is closer in free energy to the fluid phase.

Figure 7 shows the results of our cluster analysis for two distinct nuclei of size $n = 100$ and $n = 200$. The picture shows the variation of the structural signature corresponding to the distance from the center of the mass of the nucleus. The results shown in this figure are valid for $\kappa = 10$ and $\beta\epsilon = 8$. These results correspond to the points in the phase diagram where the preference for the fcc structure is strongest. The core of the cluster of size $n = 100$ has a clear bcc signature, whereas the fcc phase does not seem to play a role. However, for the larger nuclei ($n = 200$), the core of the nuclei becomes fcc-like, whereas the

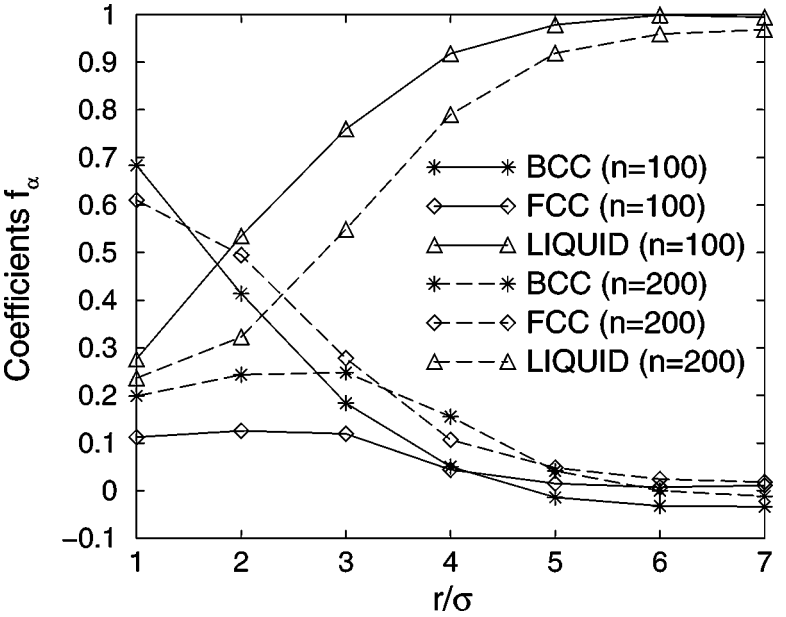

Figure 7 Structure analysis of two independent crystal nuclei of size $n = 100$ and 200 from the simulations with parameters $\beta\epsilon = 8$ and $\kappa = 10$. The figure shows the results for the fit parameters of the local bond-order analysis as a function of the distance from the center of the mass of the nuclei. The core of the cluster of size $n = 100$ has a clear bcc signature, where the cluster of size $n = 200$ shows a clear fcc structure.

bcc phase seems to disappear. Here, the cluster transformation happened before it could reach critical size. This phase transition in the precritical nucleus allows us to quantify what value of the bcc-fluid interfacial free energy is needed to compensate for the difference in the chemical potential of the two bulk structures. From our free-energy calculations, $\mu_{bcc} - \mu_{fcc} = 0.082(\pm 0.01)k_BT$. We used the CNT expression for the barrier height to estimate the fcc-liquid interfacial free energy: $\gamma_{fcc} = 0.45k_BT/\sigma^2$. The transformation from bcc to fcc nuclei occurred for $n \approx 100$. At that point, the gain in bulk free energy is $100 \times 0.082 = 8.2k_BT$. This free-energy gain must be compensated by the increase in surface free energy as the crystallite transforms from bcc to fcc. To estimate this surface free energy, we need to know the radius of the crystal nucleus for $n = 100$. If we assume that the nucleus is spherical and that the solid is effectively incompressible, we arrive at the estimate $\gamma_{bcc} = 0.38k_BT/\sigma^2$. We found such a precritical transformation from bcc to fcc for $\beta\epsilon = 2$ with $\kappa = 5$, and for $\beta\epsilon = 8$ with $\kappa = 10$ and 3.33333. In all other cases ($\beta\epsilon = 6, 8, 20$ with $\kappa = 5$), even the critical nuclei had a strong bcc signature.

6. PHSA-COATED PMMA PARTICLES

Our findings for the weakly charged colloids suggest that even a slight "softness" of the intermolecular potential has important consequences for the crystallization behavior. This effect can be relevant for experimental hard-sphere colloids, as these particles are, in fact, slightly soft. A particularly popular experimental hard-sphere colloid consists of a polymethylmethacrylate (PMMA) core coated with a thin layer of poly-12-hydroxystearic (PHSA). Because of the coating, the particles are slightly soft. We studied the effect that such a softness has on the phase behavior and the crystallization kinetics of these particles (68). In our simulations, we used an interaction potential extracted from the surface force measurements of that system (69, 70). This potential is characterized by two parameters, the thickness and the density of the PHSA layer. We found that the freezing density measured in the experiments corresponded to a layer thickness that is approximately twice as large as the thickness measured in the surface force experiment. This discrepancy may be attributed to a slight charge on the particles. On the basis of a comparison between the experimental and numerical results, we estimated that only a very small charge (less than one electron per sphere) was needed to account for the discrepancy. More recent experiments by Bryant et al. (71) indicated that the polymer layer thickness is even smaller, which suggests that the charge may even be higher. Depending on the nature of the suspension, PHSA-coated PMMA particles also exhibit long-range forces (72).

For the crystallization kinetics, we found that the nucleation rate is increased by two orders of magnitudes at constant $\Delta\mu$. This cannot account for the discrepancy between the nucleation rates observed in experiments and simulations.

7. WALL-INDUCED CRYSTALLIZATION

Thus far, we have focused on the homogeneous nucleation in colloidal suspensions. However, in the real world, crystallization is usually initiated by heterogeneous nucleation. If ice could only form through homogeneous nucleation, the freezing of water would be a rare phenomenon in countries with moderate climates.

To study the effect of an external surface on the crystallization process, we studied the behavior of monodisperse hard-sphere colloids near a plane hard wall (73). Depending on the nature of the surface, this behavior may have different effects on the freezing transition. One possibility is that the crystal phase "wets" the surface: Here, one or more crystalline layers form at the surface before the bulk freezing transition. Alternatively, the crystal may partially wet the wall, in which case crystal nucleation from a supersaturated solution takes place at the wall, rather than in the bulk.

The effect of a structured surface on the crystallization of hard-sphere colloids has been extensively studied in experiments (74–77). These experiments indicate that crystallization on a template is induced at densities below freezing. Computer

simulations by Heni & Löwen (78) of hard spheres in contact with a patterned substrate support this finding. These simulations indicate that surface freezing already sets in 29% below the coexistence pressure. Furthermore, the effect of a surface on crystallization has also been studied in mixtures of binary hard spheres (79, 80) as well as colloid polymer (81–83). In both systems, surface crystallization took place before bulk fluid-solid coexistence. In the systems studied in References 79–83, depletion forces favored the accumulation of the larger component on the wall, and this facilitated surface crystallization (84).

For pure hard-sphere systems confined by flat walls, it is not a priori clear if bulk freezing is preceded by surface crystallization. Yet, we are not aware of any systematic experimental studies of surface crystallization in pure hard-sphere systems. Courtemanche & van Swol (85) reported a numerical study of a (rather small) one-component hard-sphere system, confined between two plane hard walls. These simulations suggested that surface crystallization occurred at a pressure some 3% below the coexistence value.

Before we present the simulation results, we briefly discuss the effect that a wall has on crystal nucleation in the context of CNT. Turnbull (86) extended CNT to heterogeneous nucleation of a crystal that forms on a plane substrate. The difference between this and the homogeneous case is that now two interfaces are present. The Gibbs free energy of a crystal containing n particles is given by

$$\Delta G(n) = n\Delta\mu + A_{ws}(\gamma_{ws} - \gamma_{wl}) + A_{ls}\gamma_{ls}, \qquad (17)$$

where the subscripts w, l, and s refer to the wall, the liquid, and the solid, respectively. In this formulation, the contribution to $\Delta G(n)$ attributable to the line tension is neglected. The dependence of the interfacial free energy on the surface orientation is also ignored. Depending on the values for the interfacial free-energy densities, we distinguished the three different cases mentioned above. For the hard-sphere system, we can speculate what scenario should apply, as all relevant surface free energies have been estimated numerically (7, 87), at least at coexistence. These numbers suggest that the $\{110\}$ plane will not attach to the wall. In contrast, the $\{100\}$ planes are expected to partially wet the wall. For the $\{111\}$ plane, the situation is not as clear. The values for the surface tensions are such that the $\{111\}$ plane is expected to be at, or very close to, complete wetting.

To explore the pathway for wall-induced crystallization, we performed Monte Carlo simulations in the constant normal-pressure ($NP_\perp T$) ensemble. The simplest way to detect prefreezing is to measure the density profile of the particles between the two walls. If crystallization at the wall had taken place, it would have caused a pronounced dip between the first and second peak in the density profile. No such behavior was observed, even at pressures well above the coexistence pressure $P^*_{coex} = 11.57$ (the pressure is expressed in units of the particle diameter σ and the thermal energy k_BT: $P^* = P\sigma^3/k_BT$.) (Below, we omit the asterisk.) The situation changed when the excess pressure was increased to $\Delta P = P - P_{coex} = 0.63$. The liquid started to crystallize. These results indicated that supersaturation is needed to induce crystallization. Yet, the degree of supersaturation needed to

induce nucleation is very small compared with that typical for bulk systems. In fact, in simulations of homogeneous systems of comparable size, the rate of crystal nucleation during a simulation of similar length is negligible up to excess pressures that are an order of magnitude larger [$\Delta P \approx 5.4$ ($\phi \approx 0.53$)]. To identify the early stages of crystal nucleation, we used a local bond-order analysis (31) to distinguish between particles with a liquid-like and those with a solid-like local environment. Only a few small crystalline clusters can be identified. These clusters form and break up spontaneously. Under the same conditions, not a single solid-like cluster formed in the bulk of the fluid.

A more quantitative measure of the effect of the surface on crystal nucleation was obtained from a direct calculation of the crystal-nucleation barrier. The results for the free-energy barrier calculated at a pressure $\Delta P = 0.53$ is shown in Figure 8. At this pressure, the estimated barrier height is $\Delta G^* = 16 k_B T$ at a critical cluster size $n_c = 150$.

We can compare this estimate with a prediction for the barrier height in a homogeneous system. For the hard-sphere colloids discussed above, given the correct value for the interfacial free energy, CNT describes the barrier height quite well

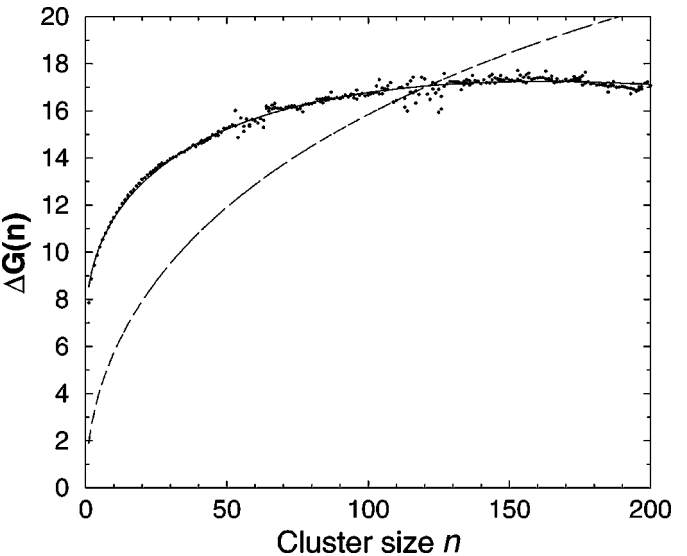

Figure 8 Calculated nucleation barrier $\Delta G(n)$ of a crystal nucleus formed at the wall as a function of its size n (*filled dots*). In the figure, we show two fits to the nucleation barrier: The dashed curve assumes the published values for the surface free energies and uses a curvature-independent line tension. To obtain the drawn curve, we used γ_{wl} as a fit parameter, and we assumed that the line tension was curvature-dependent. If we had used the CNT expression (Equation 17), there would not be a nucleation barrier at this supersaturation.

(31). But we also found that the interfacial free energy depends on density. Because the present system is close to coexistence, we used its average coexistence value $\gamma_{av} = 0.61 k_B T/\sigma^2$ (7). We then obtained $\Delta G^*_{CNT} = 1334 k_B T$ at a critical cluster size of $n_c = 52,000$. The overall reduction of the nucleation barrier attributed to the plane wall was approximately two orders of magnitude, resulting in a huge [$\mathcal{O}(10^{570})$] increase in the nucleation rate. The computed nucleation rate per unit area was $\sim 10^{-9}$ (in units D_0/σ^4). The implication for experiments is that crystallization of suspensions of hard-sphere colloids can proceed heterogeneously whenever a sufficiently flat surface is available. Yet, somewhat surprisingly, no systematic experimental observations of surface-induced freezing in hard-sphere colloids exist to our knowledge, even though most bulk crystallization studies are performed in containers with effectively flat walls.

When we compared the computed nucleation barrier with the predictions of CNT (Equation 17) we found that this expression seriously underestimated the height of the nucleation barrier. In fact, CNT predicts that, at an excess pressure $\Delta P = 0.53$, where $\Delta\mu = -0.05 k_B T$ (32), the barrier to nucleation is negligible compared with $k_B T$. To resolve this discrepancy, we are forced to take into account the line tension τ_{Line} of the crystal nuclei on the wall. If we attempt to fit our numerical data to Equation 17 including a term attributable to line tension, we can reproduce a nucleation barrier with the same height as that found in the simulations, but the shape of the simulated barrier is reproduced rather poorly (see Figure 8). A much better fit can be obtained by allowing γ_{wl} to vary within the bounds set by the large estimated error in the computed value: $1.99(\pm 0.18) k_B T/\sigma^2$. In addition, we have to allow for a curvature correction of the line tension: $\tau_{Line} = \tau_\infty + c/R$. This fit yields $\tau_\infty = 0.43 k_B T/\sigma$, $c = 1.1 k_B T$, and $\gamma_{wl} = 2.016 k_B T/\sigma^2$. With this value of γ_{wl}, the condition for complete wetting is satisfied $\gamma_{ws} + \gamma_{sl} - \gamma_{wl} = -0.02 k_B T/\sigma^2$. This agrees with the conclusion of Reference 85. However, the statistical inaccuracy in this estimate is appreciable. We can obtain a rough estimate of τ_∞ by assuming that the contribution to the free energy attributable to line tension is really nothing but the surface free energy of the lateral surface of a cylinder of height 1σ. Assuming that the lateral surface free-energy density is equal to approximately $\gamma_{ls}^{(110)}$, our estimate for τ_∞ is $\tau_\infty \approx 0.64 k_B T/\sigma$, which is within 50% of the numerical result. An estimate of the curvature correction to τ_{Line} would be even cruder.

From the simulations we can also determine the orientation and shape of the incipient crystal nucleus. Figure 9 shows a snapshot of a critical nucleus containing 150 particles. The figure also clearly shows that the $\{111\}$ plane attaches to the wall. The critical nucleus is quite flat. Clearly, small nuclei prefer to spread on the surface rather than to grow into the bulk. This is in agreement with the CNT predictions made where the $\{111\}$ face completely or nearly completely wets the wall. The fact that the range of metastability becomes very narrow provides a powerful tool for determining the freezing density in experiments. Using confocal microscopy, detecting the formation of crystallites on a flat surface should be possible. Provided the interaction of the particles with the wall is the same as the interparticle

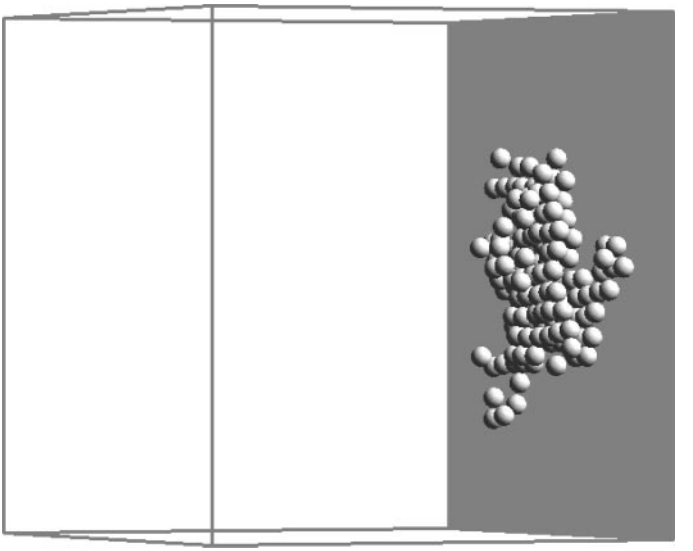

Figure 9 Sideview of the snapshot of a crystal nucleus of size $n = 150$.

potential, such crystallites will be observed first under conditions where the bulk density differs less than 1% from its value at coexistence. Our simulations suggest that prefreezing first occurs at a pressure that is approximately 2% below the coexistence pressure, but, as explained above, this estimate is subject to a large statistical uncertainty.

8. CONCLUDING REMARKS

Computer simulations of crystal nucleation play a dual role. On the one hand, they can be used as a direct test of existing nucleation theories, and on the other hand, they can be compared directly with experiments (provided we have a good model for the experimental system). The fact that both types of comparisons lead to discrepancies is interesting. The discrepancies suggest that the existing nucleation theories may need to be improved, and they indicate that there is something wrong with our interpretation of nucleation experiments. There may be a problem with our model or with our assumptions about the experimental conditions of steady-state homogeneous nucleation. Of course, there also may be problems with our numerical approach. We consider the latter possibility here. As we discussed above, there is a certain degree of arbitrariness in the choice of the order parameter that measures crystallinity. Therefore, the reported size of the crystal nuclei should be taken with caution. However, as long as the real size of the nucleus is related linearly to the computed size, the height of the nucleation barrier is not affected by

a different choice of order parameter. Any estimate of the surface free energy that is based on this height is, therefore, also insensitive to the choice of order parameter. However, if we use the complete shape of the nucleation barrier to compute the surface free energy, then we may find that the results depend on the choice of order parameter. In fact, this is not surprising, as the surface free energy of a spherical object necessarily depends on our choice of the location of the surface (e.g., surface of tension or equimolar surface). Finally, the nucleation rate should not depend at all on our choice of order parameter: This is a true, physical observable that cannot depend on the scheme that we use to compute it.

The classical theory of nucleation is, in essence, a macroscopic theory. However, at the microscopic level, such a description is not adequate. All observable quantities should be expressed as functions of material properties that are, themselves, unambiguously observable.

ACKNOWLEDGMENTS

We gratefully acknowledge Alfons van Blaaderen for helpful discussions and for a critical reading of the manuscript. The work of the FOM Institute is part of the research program of the Dutch Foundation for Fundamental Research on Matter and is made possible by financial support from the Netherlands Organization for Scientific Research.

The *Annual Review of Physical Chemistry* is online at http://physchem.annualreviews.org

LITERATURE CITED

1. Fahrenheit DB. 1724. *Philos. Trans. R. Soc.* 39:78
2. Turnbull D, Fischer JC. 1949. *J. Chem. Phys.* 17:71
3. Kelton KF. 1991. *Solid State Phys.* 45:75
4. Palberg T. 1999. *J. Phys. Condens. Matter* 11:323
5. Harland JL, van Megen W. 1997. *Phys. Rev. E* 55:3054
6. Heymann A, Stipp C, Sinn C, Palberg T. 1998. *J. Colloid Interface Sci.* 206: 119
7. Davidchack RL, Laird BB. 2000. *Phys. Rev. Lett.* 85:4751
8. Auer S, Frenkel D. 2004. *J. Chem. Phys.* 120:3015
9. Reiss H, Bowles RK. 1999. *J. Chem. Phys.* 111:7501
10. ten Wolde PR. 1998. *Numerical study of pathways for homogeneous nucleation*. PhD thesis. Univ. Amsterdam, The Netherlands. http://www.amolf.nl
11. Steinhardt PL, Nelson DR, Ronchetti M. 1983. *Phys. Rev. B* 28:784
12. van Duijneveldt JS, Frenkel D. 1992. *J. Chem. Phys.* 96:4655
13. ten Wolde PR, Ruiz-Montero MJ, Frenkel D. 1995. *Phys. Rev. Lett.* 75:2714
14. Torrie GM, Valleau JP. 1974. *Chem. Phys. Lett.* 28:578
15. Frenkel D, Smit B. 1996. *Understanding Molecular Simulations: From Algorithms to Applications*. San Diego: Academic
16. Geyer CJ, Thompson EA. 1995. *J. Am. Stat. Assoc.* 90:909
17. Chandler D. 1978. *J. Chem. Phys.* 68:2959

18. Ruiz-Montero MJ, Frenkel D, Brey JJ. 1997. *Mol. Phys.* 9:925
19. Cichocki B, Hinsen K. 1990. *Physica A* 166:473
20. Medina-Noyola M. 1988. *Phys. Rev. Lett.* 60:2705
21. Batchelor GK. 1976. *J. Fluid Mech.* 74:1
22. Cichocki B, Felderhof BU. 1988. *J. Chem. Phys.* 89:1049
23. Beenakker CWJ, Mazur P. 1983. *Physica A* 120:388
24. Tokuyama M, Oppenheim I. 1994. *Phys. Rev. E* 50:R16
25. van Duijneveldt JS, Lekkerkerker HNW. 1995. *Science and Technology of Crystal Growth*, ed. JP van der Eerden, pp. 279–90. OSL Bruinsma. Dordrecht: Kluwer-Acad.
26. Hoover WG, Ree FH. 1968. *J. Chem. Phys.* 49:3609
27. Vrij A, Jansen JW, Dhont JKG, Pathmamaoharan C, Kopswerkhoven MM, et al. 1983. *Faraday Discuss. Chem. Soc.* 76:19
28. Pusey PN, van Megen W. 1986. *Nature* 320:340
29. Schätzel K, Ackerson BJ. 1993. *Phys. Rev. E* 48:3766
30. Sinn C, Heymann A, Stipp A, Palberg T. 2001. *Prog. Colloid Polym. Sci.* 118:266
31. Auer S, Frenkel D. 2001. *Nature* 409:1020
32. Hall KR. 1970. *J. Chem. Phys.* 57:2252
33. Cacciuto A, Auer S, Frenkel D. 2003. *J. Chem. Phys.* 119:7467
34. Auer S, Frenkel D. 2001. *Nature* 413:711
35. Cheng Z, Chaikin PM, Zhu J, Russel WB, Meyer W. 2002. *Phys. Rev. Lett.* 88:015501
36. Dixit NM, Zukoski CF. 2001. *Phys. Rev. E* 64:041604
37. Volkov I, Cieplak M, Koplik J, Banavar R. 2002. *Phys. Rev. E* 66:061401
38. Cheng Z. 1998. *Colloidal hard sphere crystallization and glass transition*. PhD thesis. Princeton Univ., Princeton
39. Ostwald W. 1897. *Z. Phys. Chem.* 22:289
40. Alexander S, McTague JP. 1978. *Phys. Rev. Lett.* 41:702
41. Klein W, Leyvraz F. 1986. *Phys. Rev. Lett.* 57:2845
42. Klein W. 2001. *Phys. Rev. E* 64:056110
43. Groh B, Mulder BM. 1999. *Phys. Rev. E* 59:5613
44. Pronk S, Frenkel D. 1999. *J. Chem. Phys.* 110:4589
45. Mau SC, Huse DA. 1999. *Phys. Rev. E* 59:4396
46. Pusey PN, van Megen W, Bartlett P, Ackerson BJ, Rarity JG, Underwood SM. 1989. *Phys. Rev. Lett.* 63:2753
47. Haddon MS, Haddon SB, Poon WCK. 2001. *J. Phys. Condensed Matter* 13:553
48. Zhu J, Li M, Rogers R, Meyer W, Ottewill RH, Russel WB. 1997. *Nature* 387:883
49. O'Malley B, Snook I. 2003. *Phys. Rev. Lett.* 90:085702
50. Pusey PN. 1991. *Les Houches; Liquids, Freezing and Glass Transition*, ed. JP Hansen, D Levesque, J Zinn-Justin, pp. 764–42. Amsterdam: North-Holland
51. Kofke DA, Bolhuis PG. 1999. *Phys. Rev. E* 59:618
52. Fasolo M, Sollich P. 2003. *Phys. Rev. Lett.* 91:068301
53. Auer S. 2002. *Quantitative prediction of crystal nucleation rates for spherical colloids: A computational study*. PhD thesis. Univ. Amsterdam, The Netherlands. http://www.amolf.nl
54. Viisanen Y, Strey R, Reiss H. 1993. *J. Chem. Phys.* 99:4680
55. Oxtoby DW, Kashchiev D. 1994. *J. Chem. Phys.* 100:7665
56. Oxtoby D. 2001. *Nature* 413:694
57. Shi FG, Tong HY, Ayers JD. 1995. *Appl. Phys. Lett.* 67:350
58. ten Wolde PR, Frenkel D. 1997. *Science* 277:1975
59. Gasser U, Weeks ER, Schofield A, Pusey PN, Weitz DA. 2001. *Science* 292:258
60. Auer S, Frenkel D. 2002. *J. Phys. Condens. Matter* 14:7667
61. El Azhar F, Baus M, Ryckaert JP, Meijer EJ. 2000. *J. Chem. Phys.* 112:5121
62. Meijer EJ, Frenkel D. 1991. *J. Chem. Phys.* 94:2269
63. Dhont JKG, Smits C, Lekkerkerker HNW. 1992. *J. Colloid Interface Sci.* 152:386

64. Okubo T. 1994. *Macro-ion Characterization: From Dilute Solution to Complex Fluids*, ed. KS Schmitz, ACS Symp. Ser. 548:364. Dordrecht: Kluwer-Acad.
65. Schöpe HJ, Palberg T. 2002. *J. Phys. Condens. Matter* 14:11573
66. Wette P, Schöpe HJ, Liu J, Palberg T. 2003. *Europhys. Lett.* 64:124
67. Schöpe HJ. 2000. *Physikalische Eigenschaften kolloidaler Festkörper*. PhD thesis. Johannes Gutenberg Univ. Mainz, Ger
68. Auer S, Poon WCK, Frenkel D. 2003. *Phys. Rev. E* 67:020401
69. Costello BAD, Luckham PF. 1993. *J. Colloid Interface Sci.* 156:72
70. Costello BAD, Luckham PF, Tadros TF. 1992. *Langmuir* 8:464
71. Bryant G, Williams SR, Oian L, Snook IK, Perez E, Pincet F. 2002. *Phys. Rev. E* 66:060501
72. Yethiray A, van Blaaderen A. 2003. *Nature* 421:513
73. Auer S, Frenkel D. 2003. *Phys. Rev. Lett.* 91:015703
74. van Blaaderen A, Ruel R, Wiltzuis P. 1997. *Nature* 385:321
75. Hoogenboom JP, van Langen-Suurling AK, Romijn J, van Blaaderen A. 2003. *Phys. Rev. Lett.* 90:138301
76. Hoogenboom JP, Derks D, Vergeer P, van Blaaderen A. 2002. *J. Chem. Phys.* 117:11320
77. Hoogenboom JP, Vergeer P, van Blaaderen A. 2003. *J. Chem. Phys.* 119:3371
78. Heni M, Löwen H. 2000. *Phys. Rev. Lett.* 85:3668
79. Kose A, Hachisu S. 1976. *J. Colloid Interface Sci.* 55:487
80. Gast AP, Russel WB, Hall CK. 1986. *J. Colloid Interface Sci.* 55:161
81. Kaplan PD, Rouke JL, Yodh AG, Pine DJ. 1994. *Phys. Rev. Lett.* 72:582
82. Dinsmore AD, Warren PB, Poon WCK, Yodh AG. 1997. *Europhys. Lett.* 40:337
83. Martellozzo VC. 2001. *Crystallization and phase separationin colloidal systems*. PhD thesis. Univ. Edinburgh, Scotland
84. Poon WCK, Warren PB. 1994. *Europhys. Lett.* 28:513
85. Courtemanche DJ, van Swol F. 1992. *Phys. Rev. Lett.* 69:2078
86. Turnbull D. 1950. *J. Chem. Phys.* 18:198
87. Heni M, Löwen H. 1999. *Phys. Rev. E* 60:7057

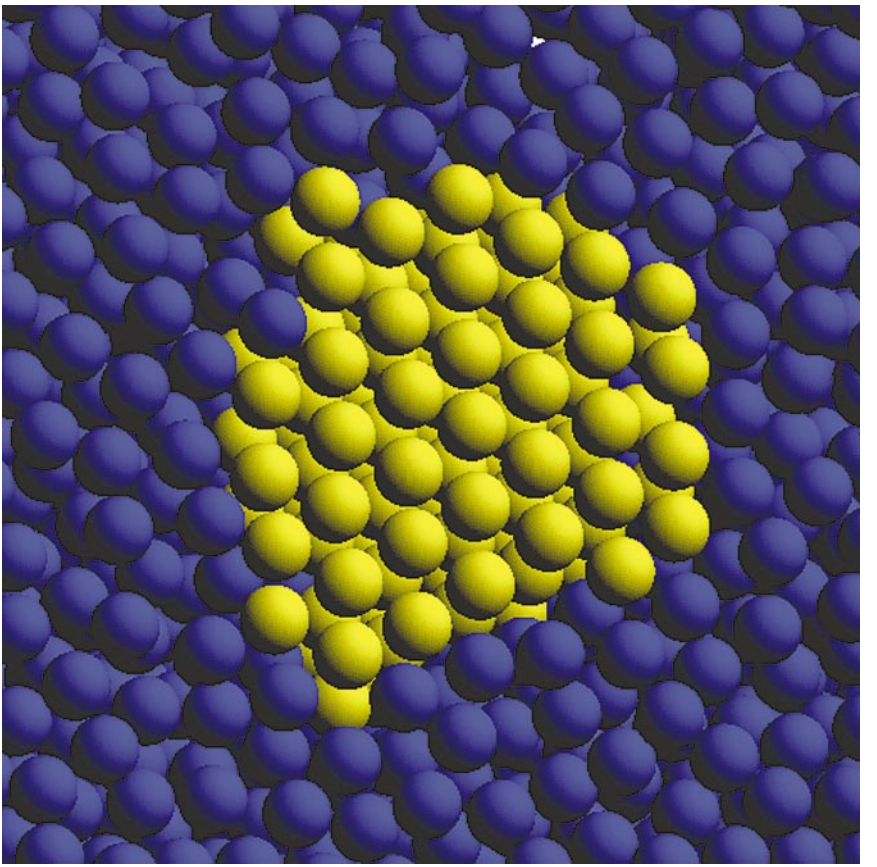

Figure 3 Snapshot of a cross section of a critical nucleus of a hard-sphere crystal at a liquid volume fraction $\phi = 0.5207$. The figure shows a three-layer-thick slice through the center of the crystallite. Solid-like particles are shown in yellow and liquid-like particles in blue. The layers shown in the figure are close-packed hexagonal crystal planes. The stacking shown in this figure happens to be fcc-like (i.e., ABC-stacking); however, analysis of many such snapshots showed that fcc and hcp stackings were equally likely.

Annual Review of Physical Chemistry
Volume 55, 2004

CONTENTS